ARTICLE   OPEN

Two different propagation patterns of spatiotemporally contiguous heatwaves in China

Ming Luo [1,2], Xiaoyu Wang[1], Na Dong[3], Wei Zhang [4], Jing Li [5], Sijia Wu[1], Guicai Ning[2,6], Lan Dai[7,8] and Zhen Liu [7,8 ✉]

Heatwaves detrimentally affect human health and ecosystems. While previous studies focused on either temporal changes or spatial extents of heatwaves, their spatiotemporal contiguity and propagation patterns are unclear. Here, we investigate the climatology, long-term trends, and interannual variations of spatiotemporally contiguous heatwaves across China during 1961 to 2018. Two distinct propagation patterns are identified by introducing a spatiotemporally contiguous events tracking (SCET) method and the k-means clustering. Type 1 contiguous heatwaves mostly generate over eastern China and move southwestward at shorter distances, while Type 2 heatwaves generally initiate over western China and move southeastward at longer distances, with stronger intensity, longer lifetime, and larger coverage. Since the 1960s, both types exhibit significant increases in frequency, intensity, coverage, lifetime, and traveling distances, with relatively larger magnitudes for Type 2, but significant decreases in moving speed only appear for Type 1. On interannual timescale, preceding winter El Niño prolongs the duration and slows down the moving speed of Type 1 through the western North Pacific subtropical high. Type 2 contiguous heatwaves are intensified by the negative spring North Atlantic Oscillation via the upper-atmospheric Rossby wave train.

INTRODUCTION

Heatwaves become a focal issue in extreme climate studies because of their severe impacts on human health, economic activities, and labor productivity[1–5]. For instance, in China, heat-induced mortality reached 26, 800 in 2019, which is around four times that in 1990[6]. Even worse, the adverse effects of heatwaves will intensify dramatically in the future because they are projected to increase considerably in terms of intensity, frequency, duration, and spatial coverage under the influence of global warming[7,8]. Heatwaves often refer to consecutive three or more days of extremely hot conditions with near-surface air temperature exceeding a certain threshold[9–11]. The evolution of heatwaves is featured with variations in both time (e.g., intensity) and space (e.g., location) during their whole lifecycles, exhibiting contiguity in three dimensions (i.e., latitude × longitude × time, see an example in Fig. 1a).

However, previous heatwave studies focused on either their temporal changes in terms of frequency, duration, and magnitude over a particular area[8,12,13] or spatial variations in terms of areal coverage during a predefined period[14,15]. Few studies considered the spatiotemporal connectivity of heatwaves and examined their co-variability characteristics over both space and time[16–19]. For example, Luo et al.[17] investigated the climatological characteristics and long-term changes of spatiotemporally contiguous heatwaves in the mainland of China during 1961–2018 based on observed daily maximum temperature (T_{max}). They adopted a spatiotemporally contiguous events tracking (SCET; Fig. 1b) method, which was introduced to identify connected components in 3D images and is termed the "cc3d" algorithm[20]. This method has also been used to track contiguous heatwaves in Australia by Reddy et al.[16] and contiguous extreme precipitation events in China by Wang et al.[21].

The main novelty of this method enables us to measure the heatwaves statistics using additional metrics in addition to frequency, intensity, duration, and areal extent, that is, evolution and/or propagation. The evolution patterns of heatwaves mainly constitute three factors, including total moving distance, moving speed, and moving direction. Albeit the importance of these metrics for heatwave propagation and early warning, they are difficult to define and remain largely unexplored in previous studies. Understanding these propagation information of heatwaves can advance our knowledge of their regular movement patterns, which can serve as more criteria to track the lifecycles of heatwaves and thus provide potential improvement of heatwave predictions. Moreover, we find a wide range of these propagation metrics, which stimulates us to separate the contiguous heatwaves into different types by distinguishing their distinct propagation behaviors using the k-means clustering method. The climatology, long-term changes, and interannual variability of different contiguous heatwave categories will be explored to shed light on their discriminative propagation behaviors. Also, previous studies have elucidated the driving role of the El Niño-Southern Oscillation (ENSO) in governing the seasonal to interannual variability of East Asian summer monsoon[22–24] and extreme weather/climate extremes[25,26]. The teleconnections of spring North Atlantic Oscillation (NAO) on East Asian summer climate have also received considerable attention in recent decades[27–29]. Thus, the possible linkages between contiguous heatwaves and ENSO and NAO are also examined and discussed in this research, which may be beneficial to making better predictions of different types of contiguous heatwaves over China and reducing their detrimental impacts.

[1]School of Geography and Planning, and Guangdong Provincial Key Laboratory of Urbanization and Geo-simulation, Sun Yat-sen University, 510006 Guangzhou, China. [2]Institute of Environment, Energy and Sustainability, The Chinese University of Hong Kong, Shatin, Hong Kong SAR, China. [3]School of Geospatial Engineering and Science, Sun Yat-sen University, 519082 Zhuhai, China. [4]Department of Plants, Soils and Climate, Utah State University, Logan, UT 84322–4820, USA. [5]College of Resources and Environment, Fujian Agriculture and Forestry University, 35002 Fuzhou, China. [6]Department of Land Surveying and Geo-Informatics, The Hong Kong Polytechnic University, Hong Kong SAR, China. [7]Center for Climate Physics, Institute for Basic Science, Busan 46241, Republic of Korea. [8]Pusan National University, Busan 46241, Republic of Korea. ✉email: zliu33@pusan.ac.kr

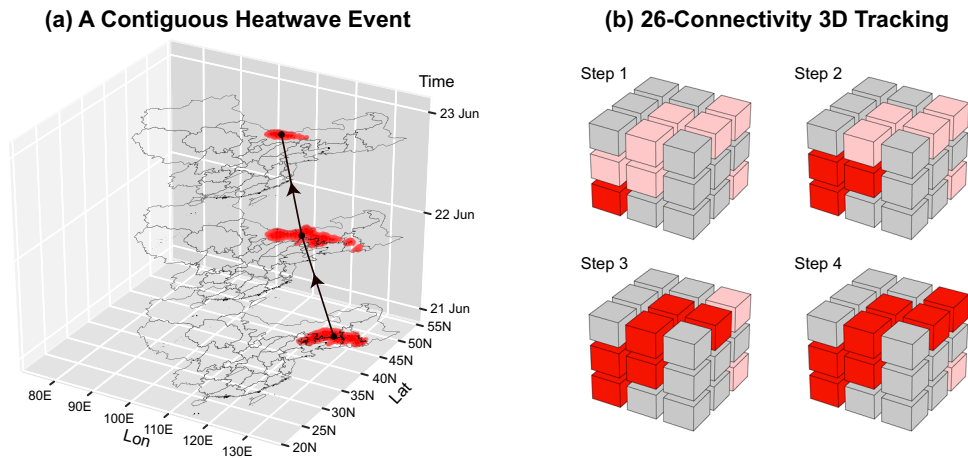## (a) A Contiguous Heatwave Event

(b) 26-Connectivity 3D Tracking

Fig. 1 Example and illustration of the spatiotemporally contiguous events tracking. a An example of a contiguous heatwave event that propagated eastward from 21 June to 23 June 1961, with black dots marking the intensity-weighted centroid throughout all participating days of the event. **b** An illustration of the 3D tracking of spatiotemporally contiguous heatwaves. Pink cell indicates that there is a heatwave day, while gray indicates not. The tracking process in **b** starts with the lower-left red cell in Step 1, and it searches the connected heatwave day in neighboring pink cells (Steps 2–4). It keeps searching until all connected cells are assigned to a contiguous event (Step 4).

Table 1. Summary of the metrics used in this study to characterize spatiotemporally contiguous heatwaves.

Category	Metric	Description
Magnitude	Total magnitude (10^6 km^2×°C)	Area-aggregated sum of the temperature exceedance relative to the threshold over all grid cells across all days of the event
	Intensity (°C)	Area-weighted average of the temperature exceedance over all grid cells across all days of the event
Area	Total area (10^6 km^2)	Sum of the areal extent of all grid cells across all days of the event
	Maximum area (10^6 km^2)	Projected area over longitude-latitude surface of the event, i.e., the potentially maximum area affected by the event
Duration	Lifetime (days)	Time interval between the beginning and end of the event (i.e., the height of the 3D contiguous heatwave structure)
	Median duration (days)	Median value of the durations of all grid cells associated with the event
Evolution	Total moving distance (km)	Sum of the centroid moving distance between adjacent time steps over the whole lifespan of the event
	Moving speed (km day^{-1})	Ratio of the total moving distance of the event to the lifetime of the event
	Moving direction	Directional angle from the centroid location of the first half of the event to the second centroid location of the event

RESULTS

Propagation patterns of contiguous heatwaves across China

Tracking contiguous heatwaves by the SCET method from a 3D perspective enables us to delineate spatiotemporal joint behaviors of heatwaves, such as moving distance, direction, and speed (see Table 1), which are not possible for previous heatwave definitions that examined either their temporal or spatial variations. Figure 3a shows the spatial distribution of 1612 identified contiguous heatwaves across China during 1961–2018 (see Methods section). The starting and ending points of the arrows denote the locations of the intensity-weighted centroid of the first and second halves of heatwaves, and the triangle and length of the vectors represent the moving direction and distance of heatwaves. There is a widespread moving distance ranging from cities to almost the whole country, indicating that the driven processes of heatwaves can be either local (e.g., urbanization[30,31]) or large-scale, e.g., the western North Pacific subtropical high (WNPSH)[12,32]. This different spatial scale feature may correspond to different lifetimes of contiguous heatwaves ranging from a few days to a month. The moving directions of contiguous heatwaves exhibit a preference of southward, particularly southeastward, which is likely related to the steering southeastward flows associated with the mid-tropospheric East Asian trough[33]. The possibly related climate

variability and circulation patterns associated with different propagation characteristics will be investigated later.

Long-term trends of contiguous heatwaves across China

We first examine the long-term trends of contiguous heatwaves across China from 1961 to 2018 in terms of frequency, intensity, total area, maximum area, lifetime, median duration, total distance, and moving speed (Fig. 2). All these heatwave metrics display significant increasing trends at the 0.05 level except for the moving speed, which decreases significantly in the study period at a rate of about 5 km day^{-1} decade^{-1}. The occurrence and intensity of contiguous heatwaves become more frequent (i.e., 1.70 events decade^{-1}) and stronger (0.02 °C decade^{-1}), respectively, consistent with previous studies that reported increasing trends in heat-waves[10,12,30]. Meanwhile, the areal extent of contiguous heat-waves expands, manifested by increases in the total area by 0.31×10^6 km^2, maximum area by 0.03×10^6 km^2, and total distance by 95.50 km in each decade. Besides, the contiguous heatwaves get a longer lifetime and duration at rates of 0.35 day decade^{-1} and 0.12 day decade^{-1}, respectively. What is worse, there is a striking decreasing trend of the moving speed by around one fourth during the past six decades. This slowdown means that contiguous heatwaves in China tend to stagnate for a longer time so that more excessive heat can be accumulated locally, which
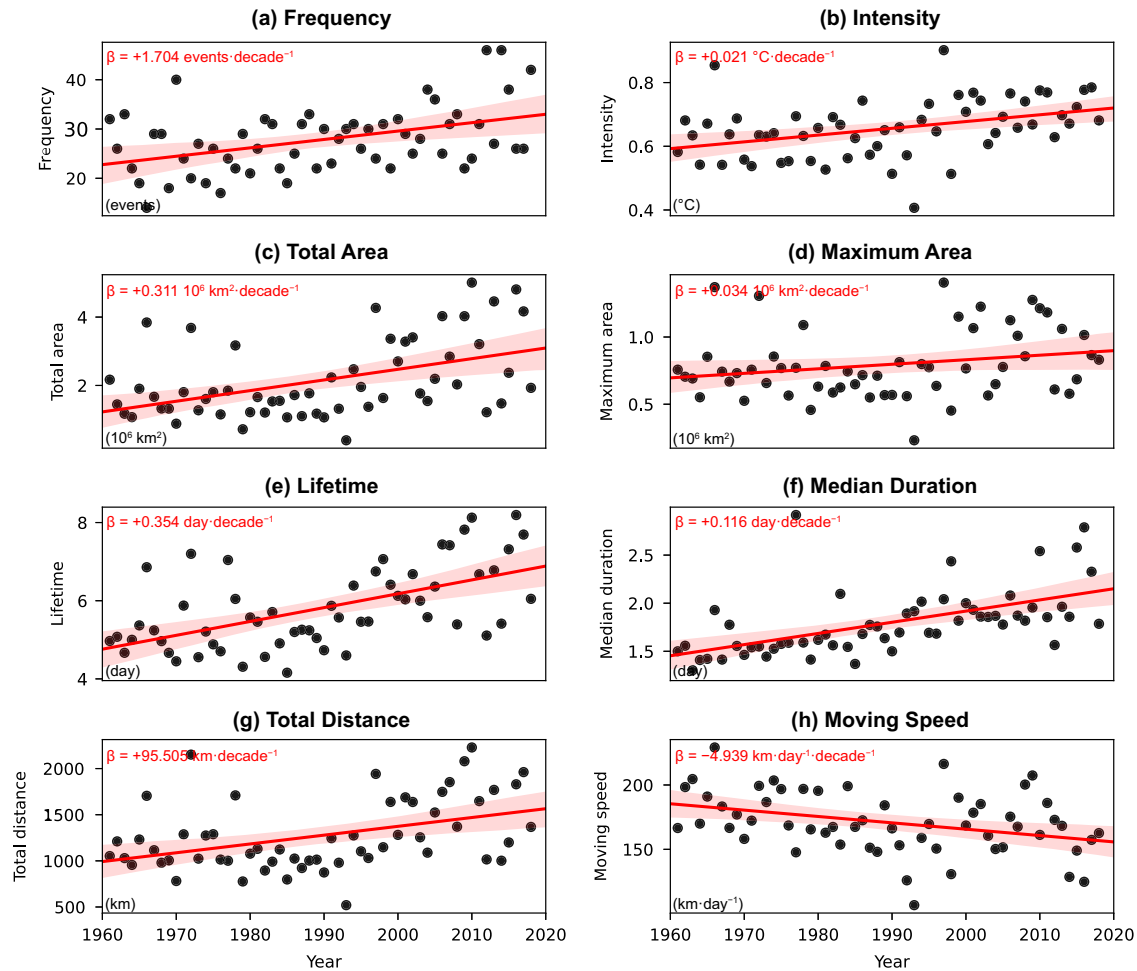
Fig. 2 Time series of the yearly statistics of the contiguous heatwaves metrics across China during 1961–2018. a Time series of the yearly frequency of the contiguous heatwave. **b–h** As (**a**) but for intensity, total area, maximum area, lifetime, median duration, total moving distance, and moving speed, respectively. The red straight line indicates the corresponding linear trend, with the red text indicating the trend magnitude. The pink shading indicates the 95% confidence interval of the fitted line. All trends are statistically significant at the 0.05 level.

may increase the potential for hazard exposure. The prolonged persistence of heatwaves is in accordance with the more-persistent synoptic weather system associated with the observed weakening trend of eddy kinetic energy[34], which may considerably exacerbate the detrimental effects of heatwaves.

Two types of contiguous heatwaves
The k-means clustering method is implemented to classify the propagation patterns of contiguous heatwaves into different regimes according to their moving directions and moving distances. We choose these two metrics as they are exclusive for contiguous heatwaves and can well reflect their concurrent evolution in both time and space. Sensitivity experiments are conducted with the clustering algorithm by perturbing the number of clusters ranging from 2 to 10, and two types of contiguous heatwaves are determined when the Sihouette Score reaches the highest[35]. The distinct differences in terms of propagation patterns and directions between the two types provide additional evidence of the rationality of the optimal cluster number chosen (Fig. 3). The majority of the contiguous heatwaves (i.e., 1439 events) fall into the first type (Type 1), which is about 8.3 times the second type (Type 2, i.e., 173 events).

Type 1 contiguous heaves are spread over the whole mainland area of China, with a relatively larger density over eastern parts (Fig. 3a). Their moving distances are much shorter than those of

Type 2, suggesting their relatively local impact. Type 1 heatwaves are apt to shift southwestwards, particularly for those that occurred over eastern China. These heatwaves are usually linked to the northwestward extension and intensification of WNPSH[36]. This intensified WNPSH is usually accompanied by reduced clouds, increased downward shortwave radiation, and associated adiabatic heating due to strengthened descending motion, contributing to more frequent and intense heatwaves[12,37]. The southwestward moving component for heatwaves over eastern China may also be relevant to the shape of the inland eastern border in association with a southwestward extension of the WNPSH, particularly near the coastline of southern China. To the west, Type 1 contiguous heatwaves show relatively sparser density over northwestern China than over eastern China. Their shorter moving distances suggest that they are mostly local processes driven. By contrast, Type 2 contiguous heatwaves are mainly situated in western China at mid-latitudes and display much longer moving distances as well as lifespan than Type 1 heatwaves. These heatwaves over northwestern China are generally related to anomalous atmospheric blockings associated with the upper atmospheric Rossby wave progression[38,39]. As a result, the prevailing propagation direction is southeastward, likely operated by the eastward movement of the Rossby wave.

To quantitively compare the differences between the two types of contiguous heatwaves, the quantile distribution of their various metrics is presented in Fig. 3b. The median values of intensity and
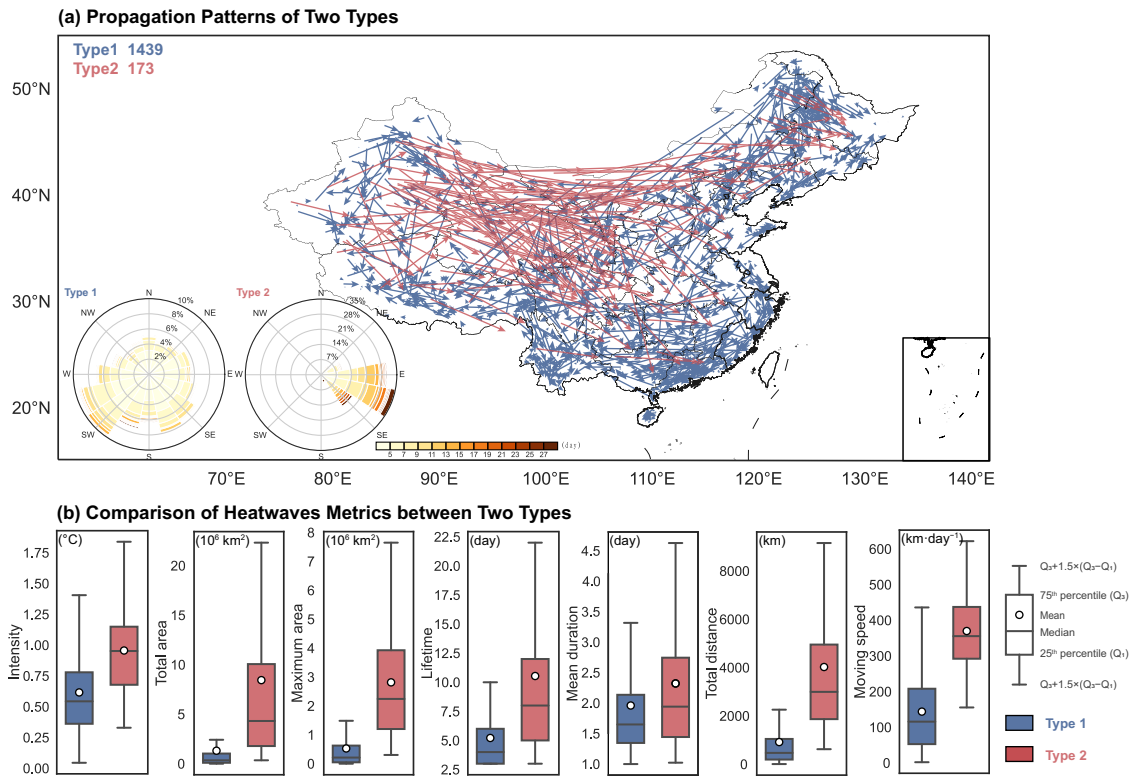
(a) Propagation Patterns of Two Types

(b) Comparison of Heatwaves Metrics between Two Types

Fig. 3 Comparison of two clustered propagation patterns of contiguous heatwaves across China during 1961–2018. a Moving patterns of two types of contiguous heatwaves. The blue arrows in **a** indicate Type 1 while the red arrows indicate Type 2 and the tail (head) of each arrow indicates the centroid location of the first (second) half of the event. The rose diagram in the lower left corner in (**a**) shows the directional distribution of lifetime of the two types. **b** Comparisons in multiple metrics between two types. The statistics in the box plots in (**b**) from the upper to lower bound represent the value of Q3 + 1.5×(Q3–Q1), third quartile (Q3), mean (circle), median (horizontal line), first quartile (Q1), and Q1–1.5 × (Q3–Q1) successively. The value of Q3–Q1 denotes the interquartile range.

mean duration for Type 2 show a positive anomaly (with respect to the grid points involved in the event) of 0.9 °C and 2.2 days, respectively. These two metrics for Type 1 are slightly smaller, i.e., 0.6 °C and 1.7 days. But the product of these two factors (i.e., intensity and duration) of Type 2 (1.98 °C × day) is nearly 2 times that of Type 1 (1.02 °C × day), which can be used to estimate the excessive heat exposed at a particular grid point covered by heatwaves. Large differences are also displayed in remained metrics. The compact range of total area, maximum area, and total distance at a relatively small magnitude for Type 1 suggests their local scales, which are likely governed by regional processes, such as urbanization, land-atmosphere interactions, and westward extension of WNPSH at the synoptic scale[12,40,41]. By contrast, the wide range of these metrics for Type 2 indicates their strong event-to-event variability. Moreover, the metric magnitudes of Type 2 are much larger than those of Type 1, i.e., around 4 times for total area, 5 times for maximum area, 2.5 times for lifetime, 5 times for total distance, and 3 times for moving speed in terms of the median values. These findings suggest that Type 2 has much stronger and broader impacts than Type 1. A good relief is the less number in the former. These distinct differences in multi-dimensional metrics further confirm the rationality of classifying the two types of contiguous heatwaves using the k-means clustering.

There is a decreasing trend in moving speed and an increasing trend in the other metrics for Type 1 (Fig. 4). The major differences between Type 1 and all types of heatwaves are that the magnitudes in the trends of total area, maximum area, lifetime, and total distance are smaller than those in total heatwaves. But note that their absolute values are also smaller for Type 1 heatwaves. Not surprisingly, by contrast, these increasing trends

are much stronger for Type 2 heatwaves due to their larger magnitudes (Fig. 5). The median duration of Type 2 increases at a rate of 2 times of that for Type 1, which will drastically intensify the extreme heat exposure (Fig. 5f). There is a slightly increasing trend of moving speed for Type 2 (insignificant at the 0.05 level; Fig. 5h).

ENSO and type 1 contiguous heatwaves

Besides the long-term trends, these metrics also exhibit considerable interannual variability, as shown in Figs. 4 and 5. Previous studies have revealed the linkages between heatwaves over Eurasia and two large-scale modes of climate variability on the interannual scale, i.e., ENSO and NAO[29,42–45]. We thus calculate the Pearson correlation coefficient of the various detrended heatwave metrics with winter Niño3.4 index and spring NAO indices. We choose the preceding winter for Niño3.4 and spring for NAO as the correlations are found to be the strongest, as suggested by previous studies[25,46]. The mean duration and moving speed for Type 1 are notably correlated with the winter Niño3.4 index, with coefficients of +0.44 and −0.43, respectively, i.e., significant at the 0.05 level (Fig. 6). This means that Type 1 heatwaves tend to last longer and move slower during El Niño/La Niña decaying years.

To further understand the physical mechanism accounting for the slower (faster) and more (less) persistent heatwaves during El Niño (La Niña) years, we regress summer geopotential height and vertical velocity onto the winter Niño3.4 index to reveal the associated atmospheric circulation patterns. The anomalous upper-atmospheric geopotential height is characterized by positive anomalies over the tropics and discernible centers over the Maritime Continent and northern Eurasia (Fig. 7a), which is accompanied by anomalous anticyclones over the western
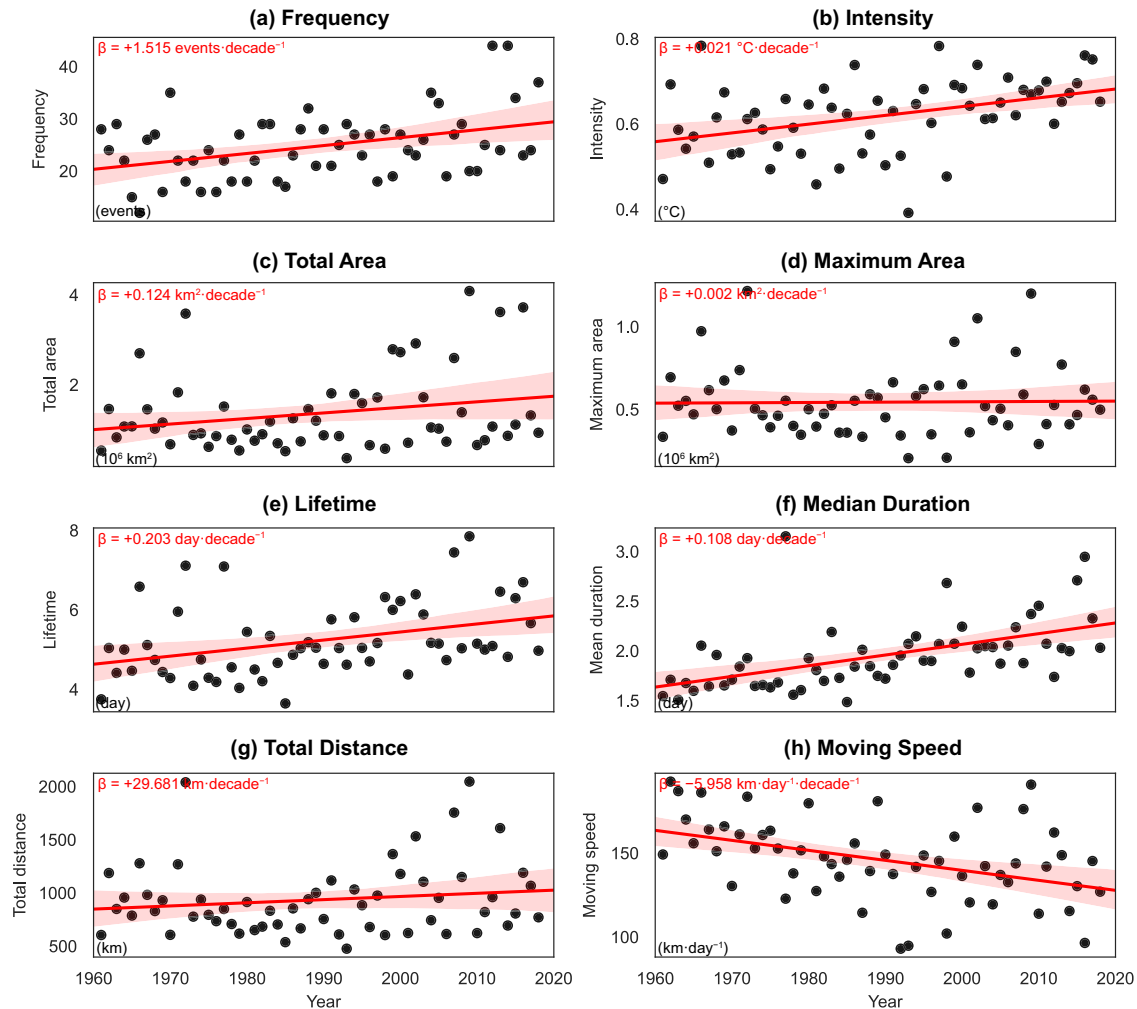
Fig. 4 Time series of the yearly statistics of Type 1 contiguous heatwaves during 1961–2018. a Time series of the yearly frequency of the contiguous heatwave. **b–h** As (**a**) but for intensity, total area, maximum area, lifetime, median duration, total moving distance, and moving speed, respectively. The red straight line indicates the corresponding linear trend, with the red text indicating the trend magnitude. The pink shading indicates the 95% confidence interval of the fitted line. All trends are statistically significant at the 0.05 level except for moving speed.

subtropical Pacific (Fig. 7b). These tropical positive anomalies of geopotential height in the upper atmosphere have been reported in previous studies as a result of the effective distribution of ENSO-induced heating in the zonal direction via fast equatorial wave propagation[47,48]. The persistence of the positive anomalies can last from the simultaneous winter to the following summer[49]. In the lower-middle atmosphere, the positive center of geopotential height anomalies moves to subtropics extending from eastern India to the central Pacific (Fig. 7c, e). The associated circulation changes are featured with a low-level anomalous anticyclone centered in the Philippines in accordance with downward motion anomalies (Fig. 7d, f), demonstrating a westward extension and an intensification of the WNPSH. This anomalous anticyclone is mainly induced by a Rossby-wave response to suppressed diabatic heating associated with western tropical Pacific cooling during ENSO events[50]. The intensified and westward shift of WNPSH is conducive to the occurrences of Type 1 heatwaves[32,51] and their southwestward movement.

NAO and type 2 contiguous heatwaves
For Type 2 contiguous heatwaves, their detrended lifetime, intensity, and total area are negatively correlated with the spring NAO index at the 0.05 significance level (Fig. 8). This means that Type 2 heatwaves are inclined to be longer, stronger and with larger affected areas if the spring NAO is at the negative phase. Previous studies have found that the tripolar pattern of sea surface temperature (SST) anomalies in the North Atlantic caused by spring NAO can persist into the following summer[52]. The teleconnections of the SST anomalies on East Asian summer climate are through exciting an anomalous wave train pattern, with positive upper atmospheric height anomalies over the Ural Mountain and the Okhotsk Sea[53]. The composite height and wind anomalies at 250 hPa are characterized by anomalous positive centers and anticyclones over the North Atlantic, the Ural Mountain, and the Okhotsk Sea, and negative centers and cyclones over western Europe and Mongolia (Fig. 9a). The composite wave activity flux (WAF)[54] differences clearly demonstrate a physical pathway from the North Atlantic to East Asia, accompanied by alternating positive and negative anomalies of the stream function (Fig. 9b). This wave train-like pattern favors the occurrences of atmospheric blockings, which suppress the intrusion of cold air and conduce to the maintenance of the anomalously high-pressure system[38]. Consequently, these large-scale circulation anomaly features contribute to the formation of stronger and larger heatwaves in the mid-latitudes (i.e., Type 2). These blocking-induced heatwaves have also been reported in European regions[39,55].
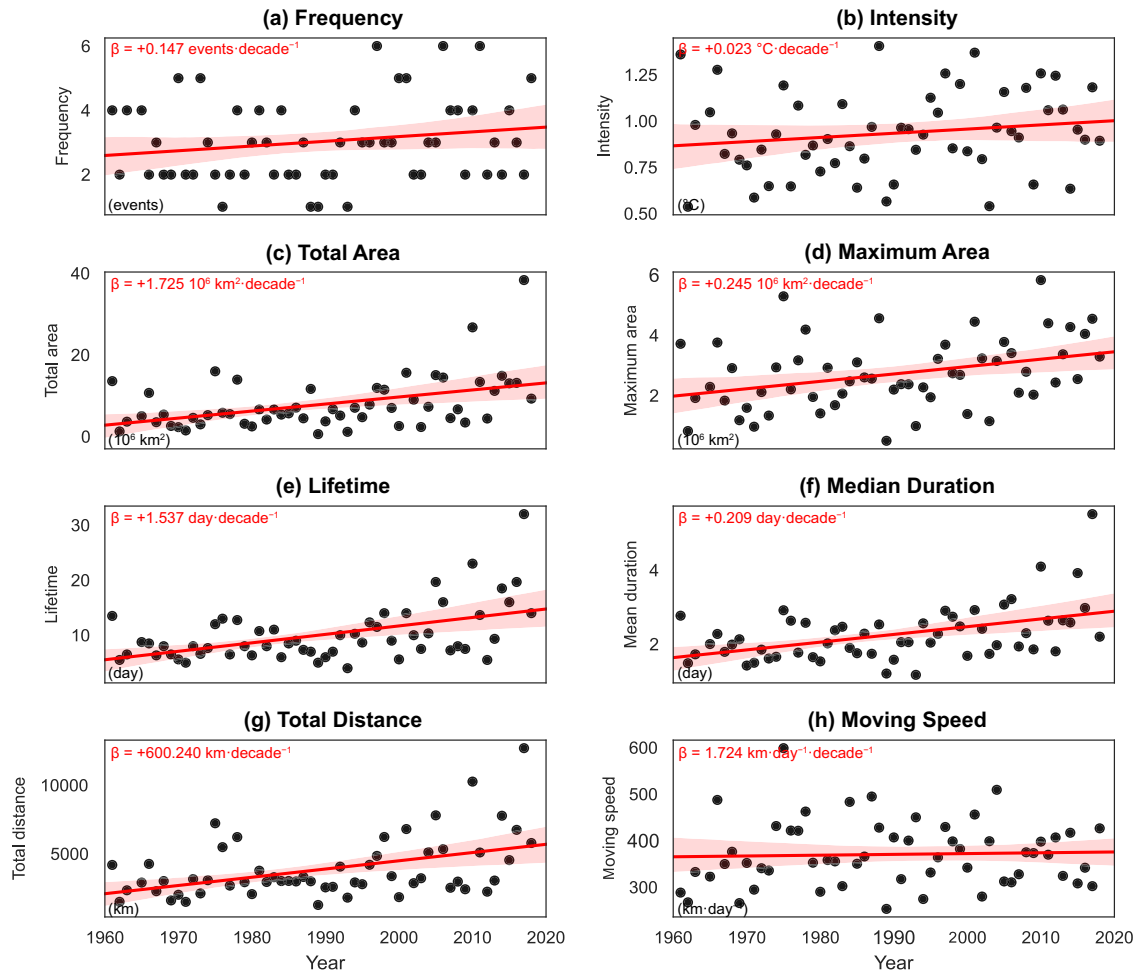
Fig. 5   Time series of the yearly statistics of Type 2 contiguous heatwaves during 1961–2018. a Time series of the yearly frequency of the contiguous heatwave. **b–h** As (**a**) but for intensity, total area, maximum area, lifetime, median duration, total moving distance, and moving speed, respectively. The red straight line indicates the corresponding linear trend, with the red text indicating the trend magnitude. The pink shading indicates the 95% confidence interval of the fitted line. All trends are statistically significant at the 0.05 level.

DISCUSSIONS

In this study, the propagation patterns of spatiotemporally contiguous heatwaves over China are investigated with the help of the SCET method, which enables us to track the moving direction, speed, and distance of individual heatwave events. The contiguous heatwaves over China display a wide range of both temporal and spatial scales, ranging from days to a month and cities to country, respectively. These heatwaves prefer to move southward (preferably southeastward), likely governed by the steering flow of the East Asian trough. All of the heatwave metrics display a significant increasing trend except for a decreasing trend in the moving speed, which means more stagnating heatwaves as global warming increases.

We further classify the contiguous heatwaves into two types based on their moving directions and distances using the k-means clustering. Type 1 contiguous heatwaves are mostly generated over eastern China and move southwestward, accompanied by the westward extension and intensification of the WNPSH. The short moving distance of Type 1 suggests their relatively local impact. By contrast, Type 2 contiguous heatwaves tend to initiate over western China and move southeastward at a longer distance associated with the eastward propagation of the Rossby wave. Compared with Type 1 contiguous heatwaves, albeit with a smaller percentage, Type 2 heatwaves have stronger intensity, longer lifetime, and larger areal extent, indicating their stronger and broader impact.

Both types exhibit an increasing trend in all metrics except for the moving speed, with larger magnitudes for Type 2 than Type 1. The moving speed shows a decreasing trend for Type 1 and an insignificant increasing trend for Type 2. On the interannual scale, the duration and moving speed of contiguous heatwaves in China are correlated with the winter Niño3.4 index for Type 1 and the spring NAO index for Type 2. During El Niño years, Type 1 heatwaves will last longer and move slower, accompanied by a westward extension and an intensification of the WNPSH in response to suppressed diabatic cooling over the eastern tropical Pacific. In the negative phase of spring NAO, Type 2 heatwaves are longer, stronger, and larger, likely related to the occurrences of atmospheric blockings associated with anomalous wave train-like patterns triggered by SST anomalies in the Atlantic.

Understanding the climatology, long-term trends, and interannual variability of contiguous heatwaves is beneficial to advancing our knowledge of heatwave covariability over both time and space dimensions on different time scales, which can be implemented for a better projection and forecast of heatwaves. Attribution of the long-term trends of contiguous heatwave metrics to anthropogenic forcing as well as quantifying their future changes also warrant further investigations to make better adaption and mitigation plans. For instance, the slowing movement of heatwaves may be caused by a wavier jet in conjunction with the weakening of the eddy kinetic energy[56]. Besides, it is of
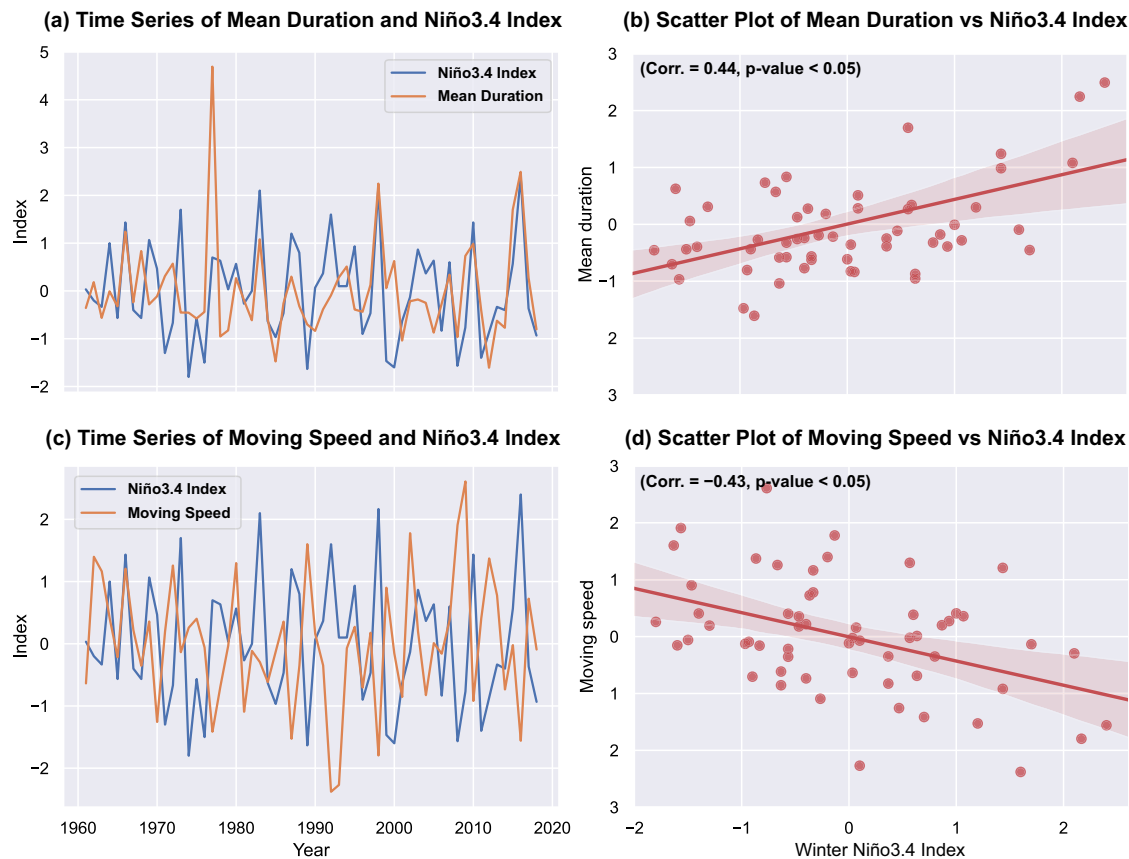
Fig. 6   Relationship between Type 1 contiguous heatwaves metrics and the winter Niño3.4 index. a, c Time series of the mean duration (**a**) and moving speed (**c**) of Type 1 contiguous heatwaves and the winter Niño3.4 index. **b, d** Scatter plots of the mean duration (**b**) and moving speed (**d**) of contiguous heatwaves versus the winter Niño3.4 index, with the straight line indicating their corresponding fitted line estimated by the simple linear regression.

great interest to include the effect of humidity, which would probably deteriorate the adverse health impact of heatwaves[57,58]. Therefore, the contiguous humid heatwaves will be investigated in future work.

METHODS
Datasets
We use gridded observational data from the CN05.1 dataset[59] (http://ccrc.iap.ac.cn/resource/detail?id=228). The dataset covers a period of 1961–2018 based on observational records of ~2400 stations in China[59]. Daily temperature in the summer season (i.e., June to August) at the 0.25° × 0.25° resolution is used in our research, which has been widely used in observational studies over China[17,60,61]. The geopotential height, horizontal wind, and vertical velocity from the NCEP/NCAR Reanalysis 1 dataset[62] are used for composite analysis to reveal the prevailing circulation patterns related to contiguous heatwaves. The Niño3.4 and NAO indices are obtained from https://origin.cpc.ncep.noaa.gov/products/analysis_monitoring/ensostuff/ONI_v5.php and https://www.cpc.ncep.noaa.gov/products/precip/CWlink/pna/nao.shtml, respectively.

Identification of spatiotemporally contiguous heatwaves
In this study, the contiguous heatwaves refer to spatiotemporal 3D heatwave events that last for a period of time and cover a certain areal extent, therefore, they are consecutive in 3 dimensions (i.e., latitude × longitude × time). In view of the spatiotemporal characteristics, the process of initiating, growing, diminishing, and terminating

can be obtained from this 3D structure. Figure 1a demonstrates the 3D structure of an eastward-moving heatwave event from June 21 to June 23, 1961 (i.e., the first case during the study period). Contiguous heatwaves are identified as clumps of adjacent heatwave grids where the daily T_{max} exceeds the corresponding 95th percentile threshold (i.e., T_{95}), which is calculated on the 15-day window over the same calendar day during a period of 30 years (i.e., 1961–1990). For each summer in 1961–2018, the gridded T_{max} values are recorded as a 3D array (see Fig. 1b for example). Then, this array is transformed into a bool array (i.e., only with "0" and "1") according to the values of T_{max} and T_{95} of each grid, where the "1" indicates a heatwave grid (i.e., $T_{max} > T_{95}$), while "0" denotes that there is no heatwave (i.e., $T_{max} \le T_{95}$).

In order to distinguish individual contiguous heatwave events, adjacent heatwave grids (i.e., "1"s in the array) are assigned the same label, using the 3-D connected component (CC3D) algorithm[20], which is implemented in a python package connected-components-3d (https://pypi.org/project/connected-components-3d[20]). In our study, a 26-neighborhood connection is employed when labeling (Fig. 1b), i.e., for the center grid on day t, 9 neighbors on day $t-1$, 8 neighbors on day t, and 9 neighbors on day $t+1$[17,21,63]. The 26-connectivity spatiotemporally contiguous events tracking (SCET) based on the CC3D algorithm takes into consideration heatwave grids that share adjacent spatiotemporal connectivity, so that the 3D evolution patterns (e.g., growing and diminishing) of heatwaves can be examined in both time and space. The 3D structure of the grid clumps with the label "1" can be connected, and the projection (e.g., on the latitude × longitude plane) can be an unbroken figure for a contiguous heatwave.

(a) Geopotential Height at 250hPa

(b) Horizontal Wind at 250hPa

(c) Geopotential Height at 500hPa

(d) Vertical Velocity at 500hPa

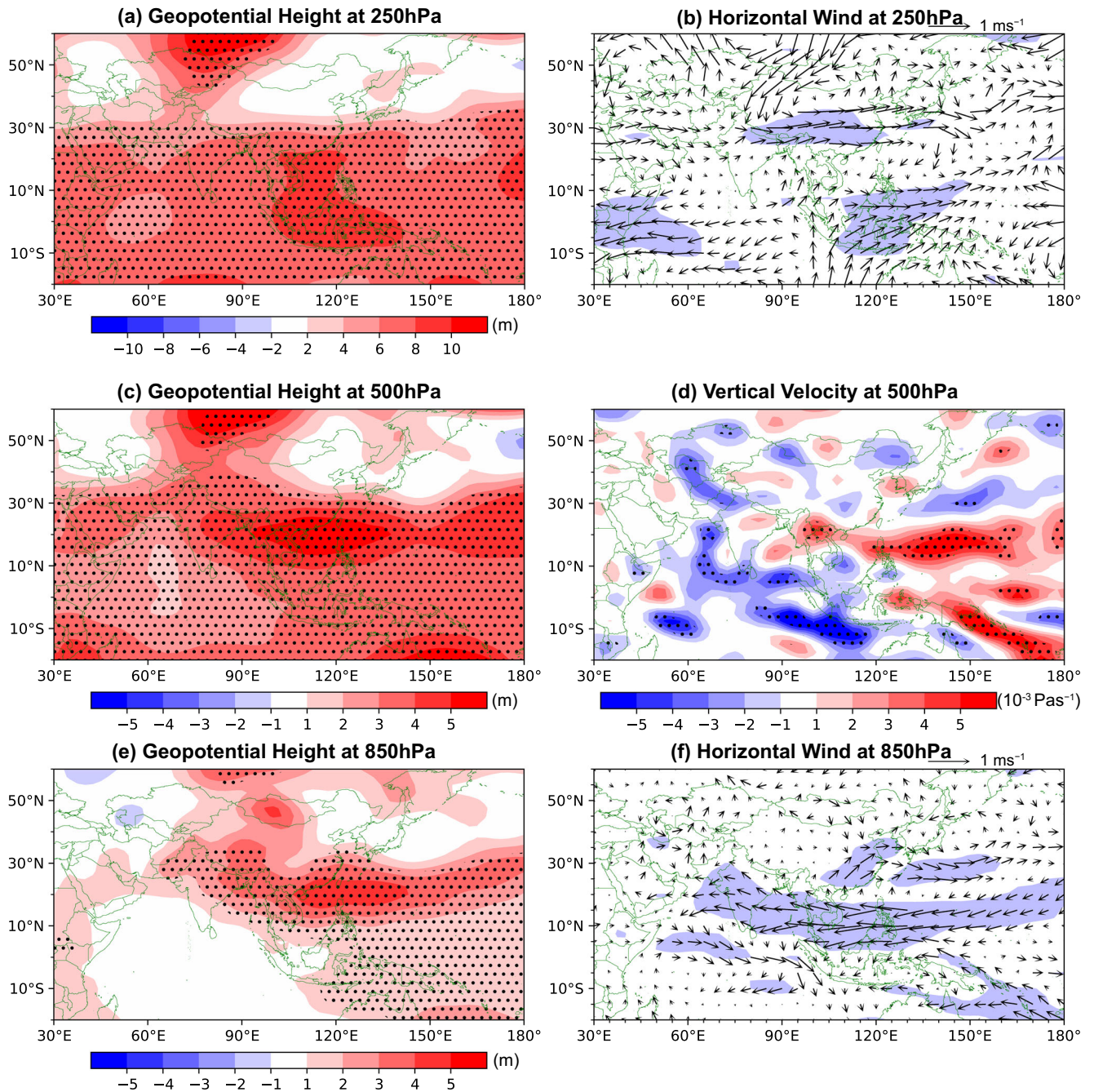## (e) Geopotential Height at 850hPa

(f) Horizontal Wind at 850hPa

Fig. 7 Summer atmospheric changes associated with the preceding winter ENSO. a, b regression of summer geopotential height (**a**) and horizontal wind (**b**) at 250 hPa onto the winter Niño3.4 index. **c, d** As (**a**) and (**b**) but for geopotential height (**c**) and vertical velocity (**d**) at 500 hPa. **e, f** As (**a**) and (**b**) but for geopotential height (**e**) and horizontal wind (**f**) at 850 hPa. Black dots in **a, c–e** indicate that the regression coefficient is significant at the 0.05 level. Light blue shadings in **b, f** denote significance at the 0.05 level for either zonal or meridional component of the horizontal wind.

Statistical methods

In our investigation, we employ five categories of the metrics of contiguous heatwaves in our research, i.e., frequency, duration, areal extent, intensity, and moving patterns as described in Table 1. The moving patterns of contiguous heatwaves are derived from the centroids of their 3D structure. The moving distance and speed are calculated according to the daily intensity-weighted average of geographical coordinates (i.e., latitude and longitude), while the direction is estimated as the displacement of the weighted centroids (i.e., divided by temporal extent) from the front to the rear half of the event[17,21]. We study all heatwave

events with a lifetime ≥3 days to include more heatwave samples in contrast to the investigation of only large contiguous heatwaves with areal extent ≥1 million km^2 in Luo et al.[17].

Simple linear regression is used to estimate the long-term trends of the multiple metrics of contiguous heatwaves in China during 1961–2018, with the statistical significance evaluated by the modified Mann-Kendall test at the 0.05 level[64]. The k-means clustering method[65] is performed to group distinct evolution patterns of heatwaves by inputting the information of moving distance and moving direction, which has the potential to forecast heatwave movements. The optimal number of clusters is determined
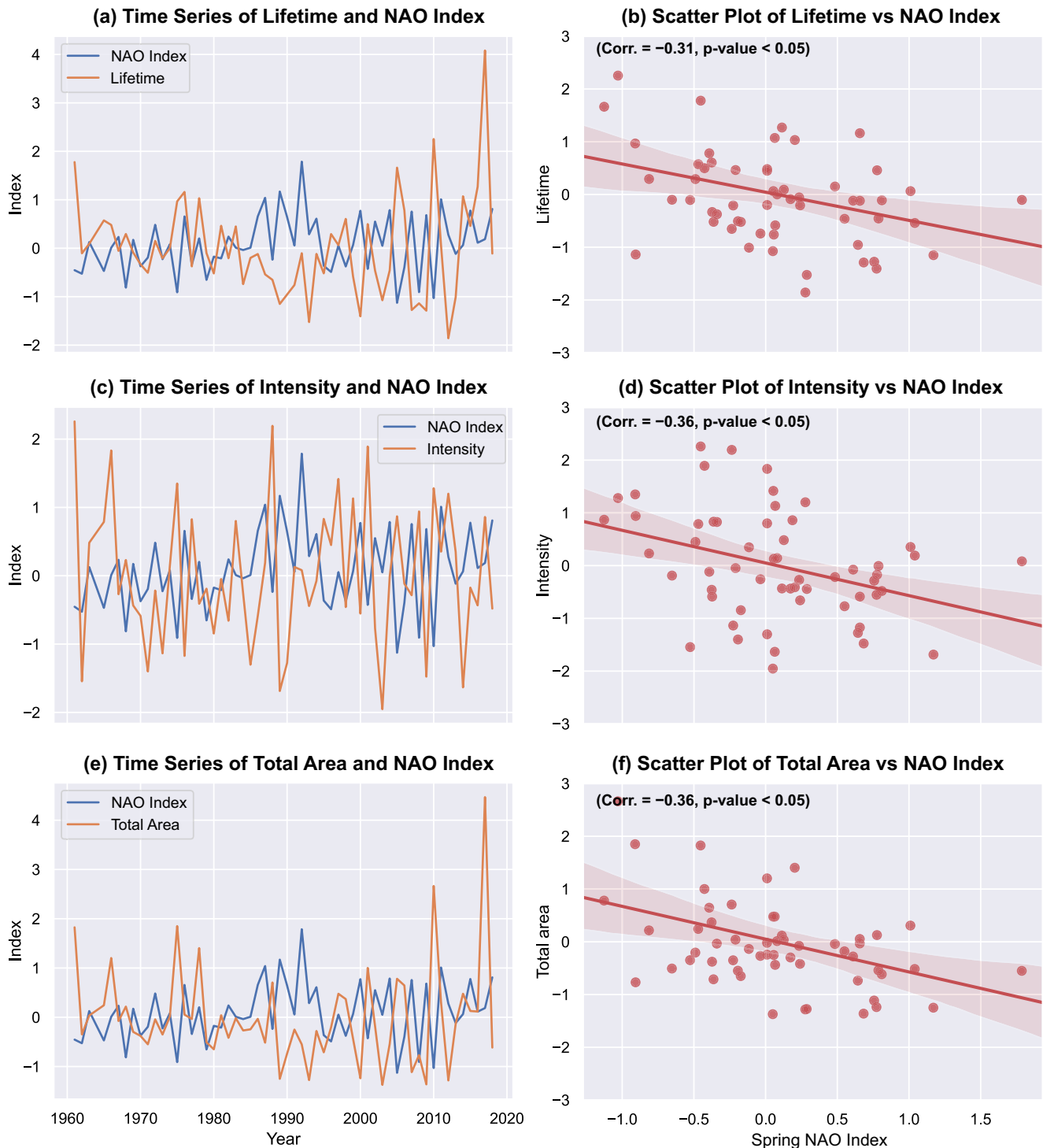
Fig. 8 Relationship between Type 2 contiguous heatwave metrics and the spring NAO index. a, c, e Time series of the lifetime (**a**), intensity (**c**), and total area (**e**) of Type 2 contiguous heatwaves and the spring NAO index. **b, d, f** Scatter plots of the lifetime (**b**), intensity (**d**), and total area (**f**) of contiguous heatwaves versus the winter Niño3.4 index, with the straight line indicating the corresponding fitted line by simple linear regression.

by the highest Sihouette Score of cluster numbers ranging from 2 to 10[35]. Comparisons of their metrics will be made to demonstrate the differences between different types of contiguous heatwaves.

To gain insight into the possible atmospheric circulation patterns related to contiguous heatwaves, regression and composite analysis associated with ENSO and NAO are examined in the fields of geopotential height, vertical velocity, horizontal wind, and the wave activity flux (WAF)[54]. The WAF vectors in pressure coordinates are calculated as Eq. 1. Ψ is 200-hPa streamfunction, u and v represent the zonal and meridional wind velocity, respectively. The overbars and primes denote the basic states and perturbations, respectively. $|\overline{U}|$ refers to the climatological horizontal wind speed. The statistical significances of the regression coefficients and composite anomalies are evaluated by
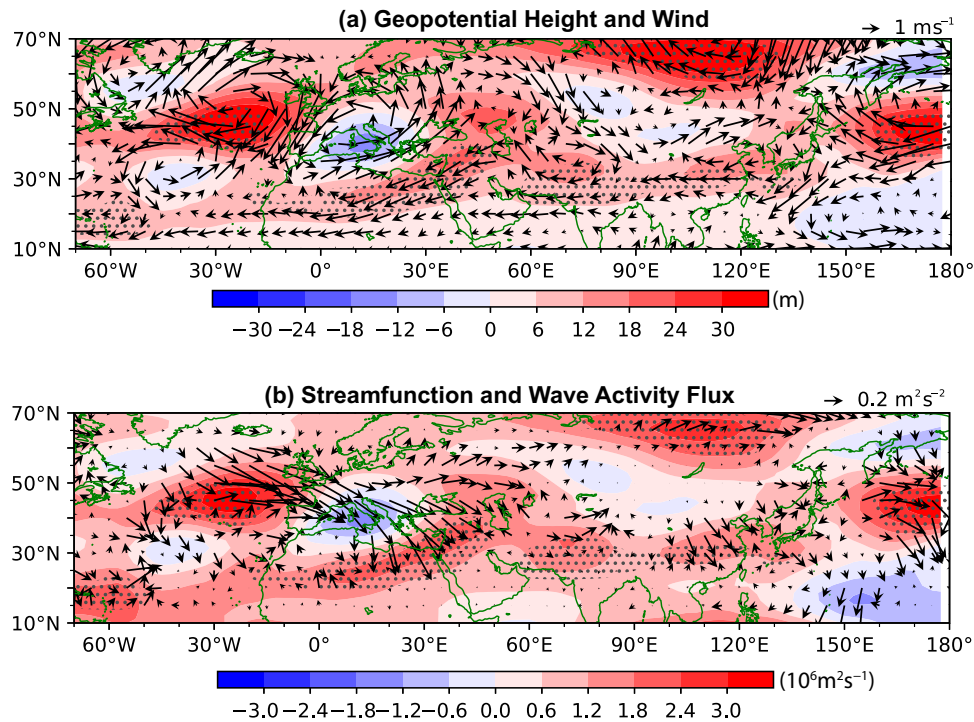
Fig. 9 Summer atmospheric changes associated with the preceding spring NAO. a Composite difference in summer geopotential height (shading) and horizontal wind (vectors) at 250 hPa between negative and positive spring NAO years (i.e., negative minus positive). **b** As **a** but for streamfunction (shading) and wave activity flux (vectors). Dotted area denotes significance at the 0.05 level.

the modified Mann-Kendall test[64] and Student's t-test, respectively.

$$
WAF = \frac{1}{2|\overline{U}|} \left\{ \begin{array}{l} \overline{u}\left[(\psi'_x)^2 - \psi'\psi'_{xx}\right] + \overline{v}\left[\psi'_x\psi'_y - \psi'\psi'_{xy}\right] \\ \overline{u}\left[\psi'_x\psi'_y - \psi'\psi'_{xy}\right] + \overline{v}\left[(\psi'_y)^2 - \psi'\psi'_{yy}\right] \end{array} \right\} \qquad (1)
$$

DATA AVAILABILITY
The CN05.1 daily gridded temperature dataset is available at http://ccrc.iap.ac.cn/resource/detail?id=228. The other meteorological data is retrieved from the NCEP/NCAR Reanalysis 1 (https://psl.noaa.gov/data/gridded/data.ncep.reanalysis.html). The Oceanic Niño Index and North Atlantic Oscillation indices are obtained from https://origin.cpc.ncep.noaa.gov/products/analysis_monitoring/ensostuff/ONI_v5.php and https://www.cpc.ncep.noaa.gov/products/precip/CWlink/pna/nao.shtml, respectively.

CODE AVAILABILITY
The source codes for the analysis of this study are available from the corresponding author upon reasonable request.

REFERENCES
1. Zander, K. K., Botzen, W. J. W., Oppermann, E., Kjellstrom, T. & Garnett, S. T. Heat stress causes substantial labour productivity loss in Australia. *Nat. Clim. Change* **5**, 647 (2015).
2. García-León, D. et al. Current and projected regional economic impacts of heatwaves in Europe. *Nat. Commun.* **12**, 5807 (2021).
3. Yang, J. et al. Projecting heat-related excess mortality under climate change scenarios in China. *Nat. Commun.* **12**, 1039 (2021).
4. Agel, L., Barlow, M., Skinner, C., Colby, F. & Cohen, J. Four distinct Northeast US heat wave circulation patterns and associated mechanisms, trends, and electric usage. *npj Clim. Atmos. Sci.* **4**, 31 (2021).
5. Ullah, S. et al. Future population exposure to daytime and nighttime heat waves in South Asia. *Earth's Future* **10**, e2021EF002511 (2022).
6. Cai, W. et al. The 2020 China report of the Lancet Countdown on health and climate change. *Lancet Public Health* **6**, e64–e81 (2021).
7. Dosio, A., Mentaschi, L., Fischer, E. M. & Wyser, K. Extreme heat waves under 1.5 °C and 2 °C global warming. *Environ. Res. Lett.* **13**, 054006 (2018).
8. Perkins-Kirkpatrick, S. E. & Lewis, S. C. Increasing trends in regional heatwaves. *Nat. Commun.* **11**, 3357 (2020).
9. Robinson, P. J. On the definition of a heat wave. *J. Appl. Meteorol. Climatol.* **40**, 762–775 (2001).
10. You, Q. et al. A comparison of heat wave climatologies and trends in China based on multiple definitions. *Clim. Dyn.* **48**, 3975–3989 (2017).
11. Perkins, S. E. & Alexander, L. V. On the measurement of heat waves. *J. Clim.* **26**, 4500–4517 (2013).
12. Luo, M. & Lau, N.-C. Heat waves in southern China: synoptic behavior, long-term change, and urbanization effects. *J. Clim.* **30**, 703–720 (2017).
13. Meehl, G. A. & Tebaldi, C. More intense, more frequent, and longer lasting heat waves in the 21st century. *Science* **305**, 994–997 (2004).
14. Sharma, S. & Mujumdar, P. Increasing frequency and spatial extent of concurrent meteorological droughts and heatwaves in India. *Sci. Rep.* **7**, 15582 (2017).
15. Mukherjee, S. & Mishra, V. A sixfold rise in concurrent day and night-time heat-waves in India under 2 °C warming. *Sci. Rep.* **8**, 16922 (2018).
16. Reddy, P. J., Perkins-Kirkpatrick, S. E. & Sharples, J. J. Interactive influence of ENSO and IOD on contiguous heatwaves in Australia. *Environ. Res. Lett.* **16**, 014004 (2021).
17. Luo, M., Lau, N.-C., Liu, Z., Wu, S. & Wang, X. An observational investigation of spatiotemporally contiguous heatwaves in China from a 3D perspective. *Geophys. Res. Lett.* **49**, e2022GL097714 (2022).
18. Wang, J. & Yan, Z. Rapid rises in the magnitude and risk of extreme regional heat wave events in China. *Weather Clim. Extremes* **34**, 100379 (2021).
19. Wang, P., Tang, J., Wang, S., Dong, X. & Fang, J. Regional heatwaves in China: a cluster analysis. *Clim. Dyn.* **50**, 1901–1917 (2018).
20. Silversmith, W. cc3d: Connected Components on Multilabel 3D Images. https://pypi.org/project/connected-components-3d/ (2021).
21. Wang, X. et al. Spatiotemporal evolution patterns of contiguous extreme precipitation events across China from a 3D perspective. *Geophys. Res. Lett.* **49**, e2022GL098840 (2022).
22. Lau, N.-C. & Nath, M. J. ENSO modulation of the interannual and intraseasonal variability of the East Asian monsoon—A model study. *J. Clim.* **19**, 4508–4530 (2006).
23. Wu, R., Hu, Z.-Z. & Kirtman, B. P. Evolution of ENSO-related rainfall anomalies in East Asia. *J. Clim.* **16**, 3742–3758 (2003).

24. Shi, H. & Wang, B. How does the Asian summer precipitation-ENSO relationship change over the past 544 years? *Clim. Dyn.* **52**, 4583–4598 (2019).

25. Luo, M. & Lau, N.-C. Amplifying effect of ENSO on heat waves in China. *Clim. Dyn.* **52**, 3277–3289 (2019).

26. Nicholls, N. et al. The El Niño–Southern Oscillation and daily temperature extremes in east Asia and the west Pacific. *Geophys. Res. Lett.* **32**, L16714 (2005).

27. Bollasina, M. A. & Messori, G. On the link between the subseasonal evolution of the North Atlantic Oscillation and East Asian climate. *Clim. Dyn.* **51**, 3537–3557 (2018).

28. Delworth, T. L. et al. The North Atlantic Oscillation as a driver of rapid climate change in the Northern Hemisphere. *Nat. Geosci.* **9**, 509–512 (2016).

29. Deng, K., Yang, S., Ting, M., Zhao, P. & Wang, Z. Dominant modes of China summer heat waves driven by global sea surface temperature and atmospheric internal variability. *J. Clim.* **32**, 3761–3775 (2019).

30. Liao, W. et al. Stronger contributions of urbanization to heat wave trends in wet climates. *Geophys. Res. Lett.* **45**, 11310–11317 (2018).

31. Luo, M. & Lau, N.-C. Increasing human-perceived heat stress risks exacerbated by urbanization in China: a comparative study based on multiple metrics. *Earth's Future* **9**, e2020EF001848 (2021).

32. Liu, Q., Zhou, T., Mao, H. & Fu, C. Decadal variations in the relationship between the western Pacific subtropical high and summer heat waves in East China. *J. Clim.* **32**, 1627–1640 (2019).

33. Lin, Z. & Bueh, C. Formation of the northern East Asian low: role of diabatic heating. *Clim. Dyn.* **56**, 2839–2854 (2021).

34. Li, N., Xiao, Z. & Zhao, L. A recent increase in long-lived heatwaves in China under the joint influence of South Asia and Western North Pacific Subtropical Highs. *J. Clim.* **34**, 7167–7179 (2021).

35. Pham, D. T., Dimov, S. S. & Nguyen, C. D. Selection of K in K-means clustering. *J. Mech. Eng. Sci.* **219**, 103–119 (2005).

36. Chen, X., Zhou, T., Wu, P., Guo, Z. & Wang, M. Emergent constraints on future projections of the western North Pacific Subtropical High. *Nat. Commun.* **11**, 2802 (2020).

37. Ding, T., Qian, W. & Yan, Z. Changes in hot days and heat waves in China during 1961–2007. *Int. J. Climatol.* **30**, 1452–1462 (2010).

38. Luo, M. et al. Observed heatwave changes in arid northwest China: physical mechanism and long-term trend. *Atmos. Res.* **242**, 105009 (2020).

39. Pfahl, S. & Wernli, H. Quantifying the relevance of atmospheric blocking for co-located temperature extremes in the Northern Hemisphere on (sub-) daily time scales. *Geophys. Res. Lett.* **39**, L12807 (2012).

40. Dirmeyer, P. A., Balsamo, G., Blyth, E. M., Morrison, R. & Cooper, H. M. Land-atmosphere interactions exacerbated the drought and heatwave over Northern Europe during summer 2018. *AGU Adv.* **2**, e2020AV000283 (2021).

41. Sun, Y. et al. Rapid increase in the risk of extreme summer heat in Eastern China. *Nat. Clim. Change* **4**, 1082–1085 (2014).

42. Wright, C. K., de Beurs, K. M. & Henebry, G. M. Land surface anomalies preceding the 2010 Russian heat wave and a link to the North Atlantic oscillation. *Environ. Res. Lett.* **9**, 124015 (2014).

43. Luo, M. & Lau, N.-C. Summer heat extremes in northern continents linked to developing ENSO events. *Environ. Res. Lett.* **15**, 074042 (2020).

44. Gao, T., Luo, M., Lau, N.-C. & Chan, T. O. Spatially distinct effects of two El Niño types on summer heat extremes in China. *Geophys. Res. Lett.* **47**, e2020GL086982 (2020).

45. Wang, W., Zhou, W. & Chen, D. Summer high temperature extremes in southeast China: Bonding with the El Niño–Southern Oscillation and East Asian summer monsoon coupled system. *J. Clim.* **27**, 4122–4138 (2014).

46. Zheng, F., Li, J., Li, Y., Zhao, S. & Deng, D. Influence of the summer NAO on the spring-NAO-based predictability of the East Asian summer monsoon. *J. Appl. Meteorol. Climatol.* **55**, 1459–1476 (2016).

47. Sterl, A., van Oldenborgh, G. J., Hazeleger, W. & Burgers, G. On the robustness of ENSO teleconnections. *Clim. Dyn.* **29**, 469–485 (2007).

48. Kucharski, F., Bracco, A., Yoo, J. H. & Molteni, F. Low-frequency variability of the indian monsoon–ENSO relationship and the tropical atlantic: the "weakening" of the 1980s and 1990s. *J. Clim.* **20**, 4255–4266 (2007).

49. Dogar, M. M., Kucharski, F. & Azharuddin, S. Study of the global and regional climatic impacts of ENSO magnitude using SPEEDY AGCM. *J. Earth Syst. Sci.* **126**, 30 (2017).

50. Wang, B., Wu, R. G. & Fu, X. H. Pacific-East Asian teleconnection: How does ENSO affect East Asian climate? *J. Clim.* **13**, 1517–1536 (2000).

51. He, B., Huang, L. & Wang, Q. Precipitation deficits increase high diurnal temperature range extremes. *Sci. Rep.* **5**, 12004 (2015).

52. Wu, Z., Wang, B., Li, J. & Jin, F.-F. An empirical seasonal prediction model of the east Asian summer monsoon using ENSO and NAO. *J. Geophys. Res.: Atmos.* **114** (2009).

53. Zuo, J., Li, W., Sun, C., Xu, L. & Ren, H.-L. Impact of the North Atlantic sea surface temperature tripole on the East Asian summer monsoon. *Adv. Atmos. Sci.* **30**, 1173–1186 (2013).

54. Takaya, K. & Nakamura, H. A formulation of a phase-independent wave-activity flux for stationary and migratory quasigeostrophic eddies on a zonally varying basic flow. *J. Atmos. Sci.* **58**, 608–627 (2001).

55. Schaller, N. et al. Influence of blocking on Northern European and Western Russian heatwaves in large climate model ensembles. *Environ. Res. Lett.* **13**, 054015 (2018).

56. Coumou, D., Lehmann, J. & Beckmann, J. The weakening summer circulation in the Northern Hemisphere mid-latitudes. *Science* **348**, 324–327 (2015).

57. Davis, R. E., McGregor, G. R. & Enfield, K. B. Humidity: a review and primer on atmospheric moisture and human health. *Environ. Res.* **144**, 106–116 (2016).

58. Raymond, C., Matthews, T. & Horton, R. M. The emergence of heat and humidity too severe for human tolerance. *Sci. Adv.* **6**, eaaw1838 (2020).

59. Wu, J. & Gao, X. A gridded daily observation dataset over China region and comparison with the other datasets. Chinese Journal of Geophysics (in Chinese with English abstract). *Chin. J. Geophys.* **56**, 1102–1111 (2013).

60. Wang, X., Lang, X. & Jiang, D. Detectable anthropogenic influence on summer compound hot events over China from 1965 to 2014. *Environ. Res. Lett.* **17**, 034042 (2022).

61. Duan, W. et al. Changes in temporal inequality of precipitation extremes over China due to anthropogenic forcings. *npj Clim. Atmos. Sci.* **5**, 33 (2022).

62. Kalnay, E. et al. The NCEP/NCAR 40-year reanalysis project. *Bull. Am. Meteorol. Soc.* **77**, 437–471 (1996).

63. Reddy, P. J., Perkins-Kirkpatrick, S. E. & Sharples, J. J. Interactive influence of ENSO and IOD on contiguous heatwaves in Australia. *Environ. Res. Lett.* **17**, 014004 (2021).

64. Hamed, K. H. & Ramachandra Rao, A. A modified Mann-Kendall trend test for autocorrelated data. *J. Hydrol.* **204**, 182–196 (1998).

65. Hartigan, J. A. & Wong, M. A. Algorithm AS 136: A k-means clustering algorithm. *J. R. Stat. Soc.: Ser. C. (Appl. Stat.)* **28**, 100–108 (1979).

ACKNOWLEDGEMENTS

AUTHOR CONTRIBUTIONS

M.L. and Z.L. designed the research. M.L. and X.W. carried out analysis. Z.L. and M.L. drafted the paper. All authors worked together on the interpretation of the results and commented on the paper.

COMPETING INTERESTS

The authors declare no competing interests.

ADDITIONAL INFORMATION

Correspondence and requests for materials should be addressed to Zhen Liu.

Reprints and permission information is available at http://www.nature.com/reprints

Publisher's note Springer Nature remains neutral with regard to jurisdictional claims in published maps and institutional affiliations.